Performance Enhancement of TSAH using Graphene and Graphene/CeO_2 -Black Paint Coating on Absorber: A Comparative Study

Kumar, Rahul
Department of Mechanical Engineering, Suresh Gyan Vihar University : Assistant Professor

Sujit Kumar Verma
Department of Mechanical Engineering, GLA University : Associate Professor

Naveen Kumar Gupta
Department of Mechanical Engineering, GLA University : Associate Professor

Santosh Kumar Singh
Department of Mechanical Engineering, United Institute of Technology : Associate Professor

KYUSHU UNIVERSITY

Performance Enhancement of TSAH using Graphene and Graphene/CeO₂ -Black Paint Coating on Absorber: A Comparative Study

Rahul Kumar[1]*, Sujit Kumar Verma[2], Naveen Kumar Gupta[2], Santosh Kumar Singh[3]

[1]Assistant Professor, Department of Mechanical Engineering, Suresh Gyan Vihar University, Jaipur, India

[2]Associate Professor, Department of Mechanical Engineering, GLA University, Mathura, India

[3]Associate Professor, Department of Mechanical Engineering, United Institute of Technology, Prayagraj,India

*Author to whom correspondence should be addressed:
E-mail: rahul.aero001@gmail.com

Abstract: The effectiveness of a triangle solar air heater can be enhanced by applying a coating on the absorber surface. The findings of comparative research of nanomaterial and hybrid nanomaterial coating on the absorber surface to improve the performance of a triangle solar air heater are presented in this article. To measure the heat transfer rate, thermal efficiency, exergy efficiency, and entropy generation the triangle solar heater is designed. Absorber plates coated with graphene and graphene/CeO₂-black paint doped into black paint in the amount of 2 % nanomaterial to enhance heat absorption. The outcomes are shown for constant air mass flow rates of 0.018 kg/s. The thermal and exergy efficiency of the graphene/CeO₂-black paint coating on the TSAH absorber plate is 3.563% and 0.55% respectively, higher than that of a graphene-black paint coating when the solar intensity is between 750 and 1220 W/m². Entropy generation is higher for graphene-black paint and lower for percent graphene/CeO₂-black paint.

1. Introduction

Drying is the oldest and most common way of preserving food that makes use of this plentiful supply of energy and has a significant economic impact across the world. In food products, there are two forms of water present: chemically bonded water and physically held water; only the physically held water is eliminated during drying. The demand for dried products is mostly due to their extended mantel piece life, product diversity, and significant volume reduction. With advances in product quality and process applicability, this may be pushed much further[1]–[3].Open-air drying/Sun-drying and mechanical dryers are the most common methods for drying agricultural products, with solar dryers being used infrequently. Since ancient times, open-air drying has been the most common, cheapest, and widely used method, and it is still used in many parts of the world, including Indian rural areas. This approach, while completely dependent on weather conditions, is labor expensive, unsanitary, unreliable, time consuming, resulting in non-uniform drying, and necessitates a vast space for spreading the food to dry, and has failed to provide expected results in certain areas.

The efficient use of solar radiation has supported emerging study disciplines such as solar thermal energy. Solar energy is the primary source of energy on the planet since it is free, renewable, and abundant. Energy is critical to a country's development. There is a considerable quantity of solar energy that can be utilized as a source of energy. As a consequence, the utilization of solar energy for human civilization has become one of the most pressing issues in the scientific community. This energy may be used in a range of methods, including various types of solar air heaters. The most outlay solar generating systems are typically SAHs. Cold weather house warming, crop drying, space heating, and wood are all popular applications for this solar energy system.

Researchers have offered several solutions to this problem. The most practical option is to coat on the absorber plate to improve the heat transfer coefficient[4]–[9]. The litérature survey is as follows, based on the nanomaterial coating on the absorber surface: CuO nanomaterials were studied for solar absorber surface coating. This experiment was carried out both indoors and outside to evaluate the solar absorber. In two and single glazing circumstances, the CuO structure's acute morphological and random distribution permitted an increase in optical broadband absorption of TiNOX absorber, with values estimated at 97 percent and 95

percent of the present state[10]. When used to coating an absorber to show certain spectrum qualities, three kinds of carbon nanotubes were compared. The P-CNT absorber's spectrum selectivity was optimized in this investigation[11]. A comparison of $Nb-TiO_2$ and $W-SiO_2$ was carried out. The $W-SiO_2$ absorber has a higher emittance. Solar emittance and absorption are 0.1 and 0.93 at 350^0 K, respectively[12]. Corrosion behavior improves as a result of the investigation. Finally, graphene particles were required to increase corrosion protection by paint dispersion to 0.05%[13]. The TSAH was shown in the experimental study with various mass flow rates and nanomaterial coatings on the absorber surface. It was observed that the BP-II absorber surface outperforms the BP-I absorber plate by 4.27 percent in terms of thermal performance[14]. Investigated absorber coatings to see which paints had the best absorption. It was observed that the glossy nickel coating enhanced efficiency and reduced heat loss and optical gain in the collector after completing the tests[15]. A coating of black paint combined with graphene nanomaterial was placed on an absorber plate in an experimental investigation on a triangle duct SAH. As a consequence, the maximum solar intensity for glass is 930-980 W/m^2, and the temperature of the absorber plates enhances thermal efficiency by around 4.9 percent[16]. The effect of graphene and copper oxide nanoparticles doped into black paint at different percentages for absorber surface coating that enhances heat transfer rate was studied. According to the findings, 0.3 percent graphene/CuO-black paint enhances thermal efficiency by 3.58 percent on average[17]. The effects of SAH absorber surface coating were investigated. The coating was made up of carbon nanotubes and cupric oxide nanoparticles. Doping commercial black paint with 4% CNTs/CuO increases overall efficiency by 24.4 percent while also raising the temperature difference by 22%[18]. The above review focoused the coating on the absorber surface enhance the performance for solar energy conversion system.

This current study aims to investigate the comparative analysis of graphene-black paint and graphene/CeO2-black commercial paint coating on absorber surfaces. In both cases, 2% nanomaterial embedded in black paint is used as a coating substance. The input air temperature and solar intensity are used as variable parameters with a constant mass flow rate. The experimental analysis on the other hand determines TSAH's thermal efficiency, heat loss component, exergy efficiency, entropy generation, length-wise inside temperature distribution, and outlet temperature. The study will enable a better understanding of the coating of the hybrid nanomaterial for the solar energy conversion system.

2. Materials and method

The influence of a newly developed absorber plate on TSAH performance characteristics is investigated using an experimental setup. The system was tested using a TSAH with various nanomaterials coated with black paint. Table 1 shows the physical dimensions of the TSAH. The triangular work section is 1 meter long. As illustrated in Fig. 1, several nanomaterial coatings were developed on the absorber surface.

Table 1. Technical specification of the TSAH.

TSAH Components	Technical specifications	Units
Length of Triangular section	1.0	m
Length of one side triangle	0.60	m
Height of triangular section	0.52	m
Hydraulic Diameter	0.352	m
The aspect ratio of TSAH	1.15	
Length of outlet and inlet section of TSAH	0.40	m
Diameter of inlet and outlet pipe	0.0635	m
Number of glazing Plates	1	
Area of glazing Plate	0.6	m^2
Area of the absorber plate	1.2	m^2
Edge area of triangular section	0.312	m^2

2.1 Experimental Installation

The experiment and arrangement were carried out at GLA University's solar research facility in Mathura (India). The schematic diagram may be seen here in Fig. 2. With a hydraulic diameter of 0.352 m and a triangle work section aspect ratio of 1.15, the triangular section has dimensions of 1m, 0.6 m, and 0.52 m. The airflow inside the triangle duct is considered to be turbulent as an assumption in the experiment. As indicated in the diagram, thermal characteristics stay constant during the test condition in Table 2. With the aid of an air-blower, the air is drawn in from the entrance section during atmospheric conditions. The pressure between the entry and exit portions was measured using a micro manometer. The solar intensity meter measures solar intensity on the glazing panel. To ensure that the pipe part was leak-free, the air blower was turned on and run for half an hour before the research began. An anemometer was used to detect airspeed and a motor controller at the output part was designed to make the hot air at the exit side. A K-type thermocouple has been used to measure the temperature of the entry and exit ports in the experimental setup. The thermocouple was linked to various locations through perforations in the surface of the absorber to reduce the influence of the wire on the tubing's flow.

Table 2.Thermo-physical properties of air.

Specification	Technical Specification	Units
Density	1.12	kg/m^3
Specific Heat at Constant Pressure	1.006	KJ/kg-k
Specific Heat at Constant Volume	0.718	KJ/kg-k
Thermal Conductivity of air	0.0262	$w/m\ K^2$
Viscosity	$1.783x\ 10^{-5}$	N/m
Constant of Ideal Gas	287	J/kg-k

Fig. 1: Experimental setup
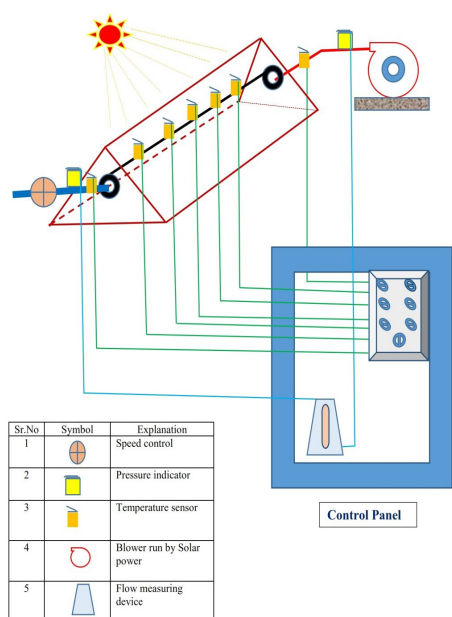
Fig. 2: A schematic diagram of TSAH

The FESEM test facilities at MANIT Jaipur (MRC) in Rajasthan were used. First, 2 percent concentrations of graphene nanomaterial are mixed into black paint applied to the absorber surface. Chemical exfoliation produces graphene, which is a thin coating of graphite. The graphene's physical characteristics are represented as soft, light, and dark fluffy black powder. The graphene nanomaterial was distributed in commercial black paint at a mass proportion of 2%. It took 30 minutes of magnetic stirring to complete. The aluminium absorber plate was then sprayed with an electric sprayer at room temperature. Fig. 3 shows FESEM Images of the absorber plate coating for graphene material, and Fig. 4 offers the analysis of the Absorber plate coating of graphene/CeO₂-black paint of FESEM image.
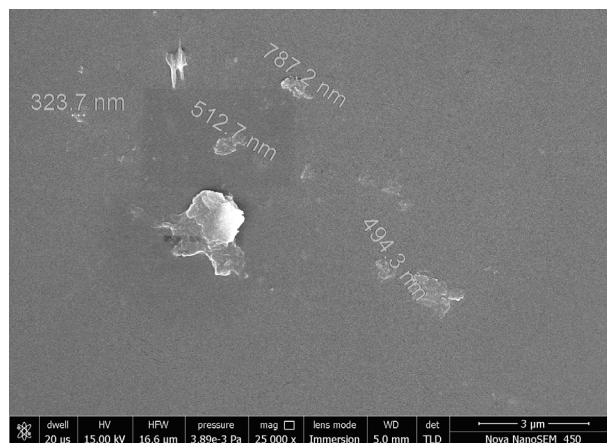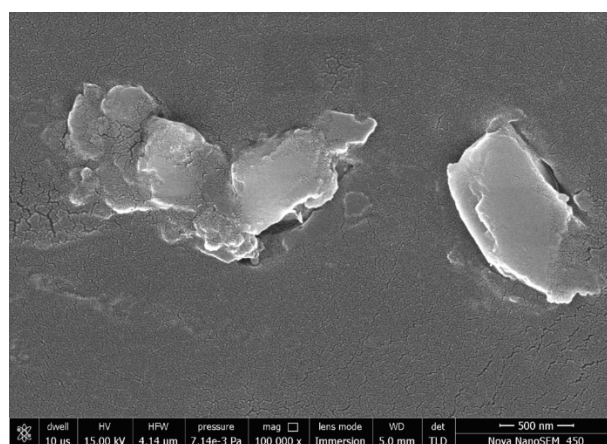

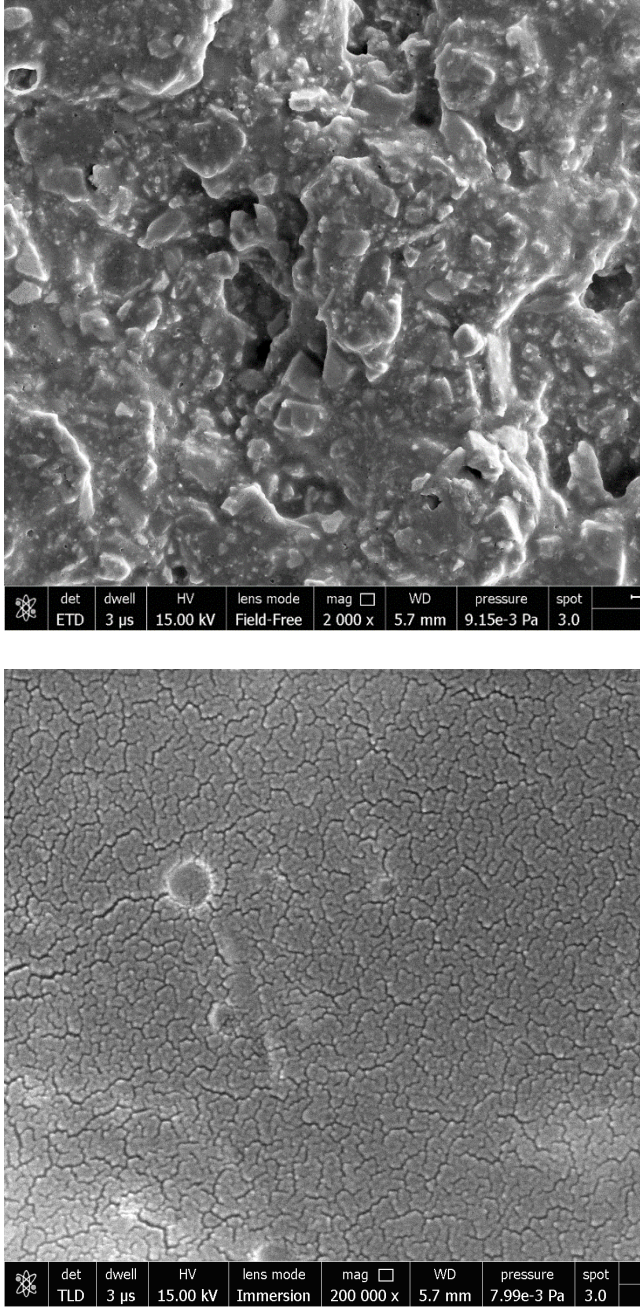**Fig. 3:** Absorber plate coating of Graphene black paint of FESEM images

Fig. 4: Absorber plate coating of graphene/CeO2-black paint of FESEM image

3. Data reduction

3.1 Performance analysis calculations

The top to down technique, which is described below, is used to compute the TSAH's performance based on data from a prior paper published in the literature. The temperature of the exit air is then determined. The preliminary temperature difference (To) is assumed to begin the analytic method.

$$T_o = T_i + \Delta\text{T}$$

The average temp for both types of absorber surface is maintained, and it is determined by the relationship. [19]

$$T_p = \frac{T_0 + T_i}{2} + 10$$

The equation was utilized to determine the heat transfer between the ambient air and the glass cover caused by convection.[20]

$$h_w = 5.7 + 3.8V$$

The average temperature of the absorber plate is used to calculate the thermal loss coefficient from the glass plate. (U_t)[21].

$$U_t$$

$$= \left(\frac{N}{\frac{C}{T_p} \left(\frac{(T_p - T_a)}{(N+f)} \right)^e} + \frac{1}{h_w} \right)^{-1}$$

$$+ \frac{\sigma(T_p + T_a)(T_p{}^2 + T_a{}^2)}{\frac{1}{\epsilon_p + 0.00591Nh_w} + \left[\frac{2N + f - 1 + 0.133\,\epsilon_p}{\epsilon_g} \right] - N}$$

$$f = (1 + 0.089h_w - 0.01166h_w\epsilon_p)(1 + 0.07866N);$$

$$e = 0.43 \left(1 - \frac{100}{T_p} \right);\ .\text{[22),23]}$$

$$C = 520[1 - (0.000051\beta^2)]\,For\ 0^0 < \beta < 70^0$$

The bottom and edge heat removal coefficients are computed using the equation below for a specific design.,[24]

$$U_b = \frac{k_i}{t_i}$$

$$U_e = U_b \left(\frac{A_e}{A_c} \right)$$

The overall coefficients of heat loss, The following equation describes U_L, which is the sum of the glass plate's edge, bottom, and loss coefficients:

$$U_L = U_t + U_b + U_e$$

The TSAH's beneficial heat gain may be measured in terms of heat energy consumed;

$$Q_{u1} = A_p \left[I(\tau\alpha) - U_L(T_p - T_a) \right]$$

The TSAH's Reynolds number and airflow rate are calculated using the equations below. [25]

$$\dot{m} = \frac{Q_{u1}}{C_p\Delta T}\ \&\ R_e = \frac{\dot{m}D_h}{\mu A_t}\ \&\ P_r = \frac{\dot{m}c_p}{k_a}$$

The following is an equation that may be used to determine the Nusselt number. [26]

$$N_u = \frac{3.66 + 0.0668(D_h/L)R_eP_r}{1 + 0.04[(D_h/L)R_eP_r]^{2/3}}$$

Nusselt number co-relation determines the convection heat transfer coefficient.

$$h = \frac{N_u k_a}{D_H}$$

The glass plate efficiency factor is calculated using the formula below. [27] as well as the heat removal factor [28];

$$F' = \frac{h}{h + U_L}$$

$$F_R = \frac{\dot{m}C_{pair}}{A_c U_L}\left[1 - exp\left\{\frac{-F'U_L A_p}{\dot{m}C_{pair}}\right\}\right]$$

The energy absorbed is computed using the equation with the heat removal factor included.

$$Q_{u2} = F_R A_p[I(\tau\alpha) - U_L(T_o - T_i)]$$

If the difference between (Q u1-Q u2) is more than 0.05 percent *Q u1, the iterative procedure changes the mean plate temperature until it is negligible. Figure 5 shows all processes of calculations. Consequently $Q_u = Q_{u1} = Q_{u2}$.

The TASH's thermal efficiency is provided by;

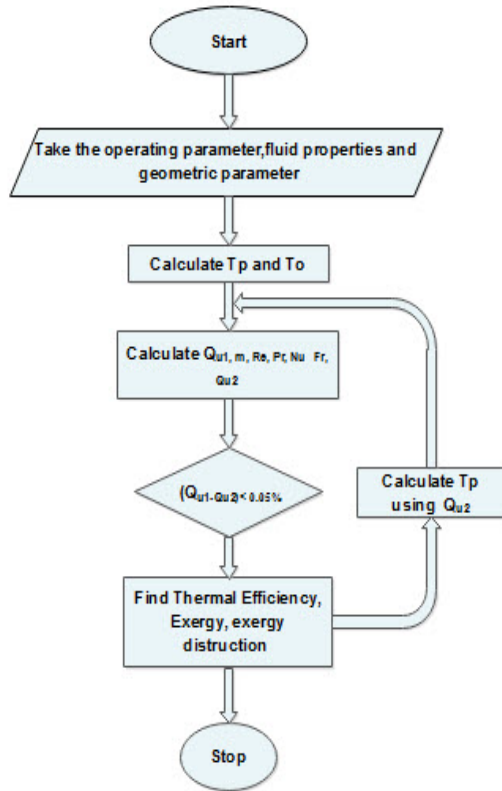$$\eta_{th} = F_R(\tau\alpha) - \frac{F_R U_L(T_o - T_i)}{I}$$

Fig. 5: Numerical parameter calculation

3.2 Exergy analysis calculations

The energy absorbed by the working fluid (air) inside a TSAH will rise as exergy destructions are reduced. The net exergy energy rate of a solar air heater is calculated as follows:

$$E_s = IA_p\left(1 - \frac{T_a}{T_{sun}}\right)$$

Exergy destructions of various types are computed as follows:

$$E_{opt} = IA_p\eta_{ex}(1 - \tau\alpha)$$

$$E_{abs} = IA_p\tau\alpha\left[\eta_{ex} - \left(1 - \frac{T_a}{T_p}\right)\right]$$

$$E_{env} = U_L A_p(T_p - T_a)\left(1 - \frac{T_a}{T_p}\right)$$

$$E_{ht} = IA_p\eta_{th}\left[\left(1 - \frac{T_a}{T_b}\right) - \left(1 - \frac{T_a}{T_p}\right)\right]$$

$$E_f = \frac{\dot{m}\Delta P}{\rho T_b}$$

Exergy is gained by the collector surface, which is depicted as,

$$E_n = IA_p\eta_{th}\eta_c - P_m(1 - \eta_c)$$

The TSAH's energy efficiency is determined by this equation;

$$\eta_{ex} = \frac{E_n}{E_s}$$

4. Results and Discussion

In this part, the key contributions of the experimental examination of the two models of TSAHs were described. The absorber plate is subjected to an experimental comparison of nanomaterials and hybrid nanomaterials.

The research was done to compare the heater's thermal performance. At the time of both trials, the sun intensity and ambient temperature were both changing. The average ambient temperature for the experiment is 306-308⁰ K. The thermal efficiency of both designs of the absorber surface of the solar heaters was enhanced by increasing the solar intensity. The thermal efficiency is increased with the solar intensity increases but thermal efficiency is almost constant at higher intensity of solar radiation. The thermal efficiency value for the graphene coating absorber plate and graphene with cerium oxide coating are shown in Fig. 6. These efficiency values were attained in the constant mass flow rate, the various value of ambient temperature, and solar intensity using the efficiency equation. We discover that as the mass flow rate of air rises, the thermal efficiency increases in every case. As a result, at higher mass flow rates, thermal energy is transferred to the air by increasing the effect of turbulence inside the examination section, which also lowers the temperature of the absorber plate. As a result, heat loss to the environment is reduced, resulting in increased thermal efficiency.
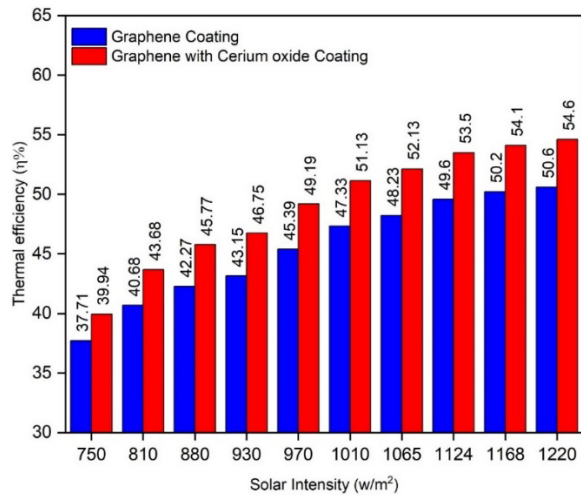
Fig. 6: Variation of solar intensity vs. thermal efficiency

Fig. 7 illustrates the variation of solar intensity vs heat loss component with graphene/CeO_2-black paint. The improvement in heat gain in the TSAH with hybrid coated absorber plate was attributable to significant absorption of incoming solar energy and heat transfer between absorber surfaces and flowing air, according to the research. The total of all losses in a triangle system produces the overall heat loss coefficient. It shows that the TSAH absorber plate with hybrid coating has the uppermost heat transfer rate and the lowermost heat loss coefficient. It determined that heat loss reduces as ambient temperature and solar radiation increased.
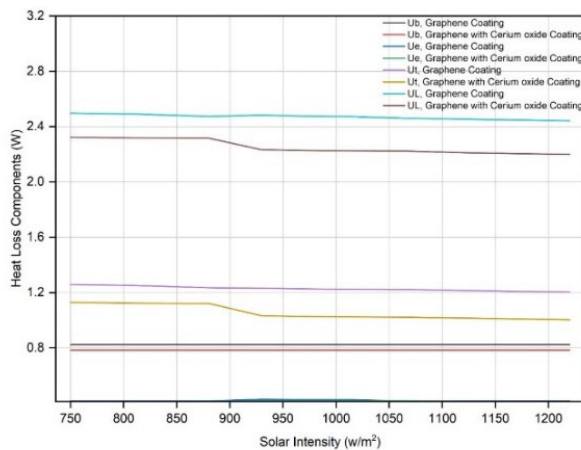

Fig. 7: Variation of solar intensity vs. heat loss components of the hybrid coating.

Fig. 8 depicts the hybrid coating's change in exergy loss components as well as solar intensity. In a TSAH's exergy study, the temperature of the absorber surface is important. As the sun intensity value rises, the exergy destruction goes up with it. This is due to the fact that the heat loss coefficients increase together with the internal duct temperature. In such conditions, the pressure loss throughout the systems is higher.
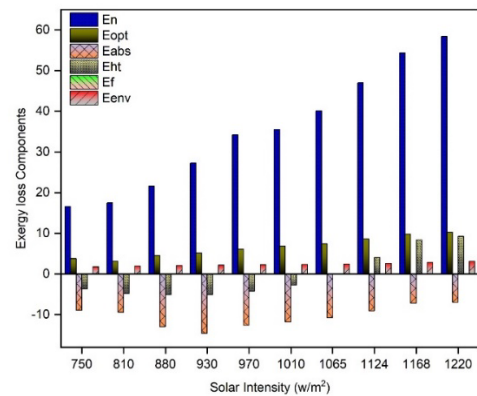

Fig. 8: Variation of exergy loss components and solar intensity for Hybrid coating

Fig. 9 shows entropy generation analysis is extremely important in the design and enhancement of the TSAH. Entropy production is the minimum requirement in any thermal system, resulting in higher thermal efficiency. Entropy production reduces as the solar intensity rises. Entropy production is the difference in temperature and pressure decrease between the entrance and exit portions because the hybrid black paint coating for the absorber surface enhances the surface area of the absorber surface and also increases the heat transfer rate, the entropy production is lower for graphene/CeO_2-black paint coating compared to graphene black paint for the same solar intensity.
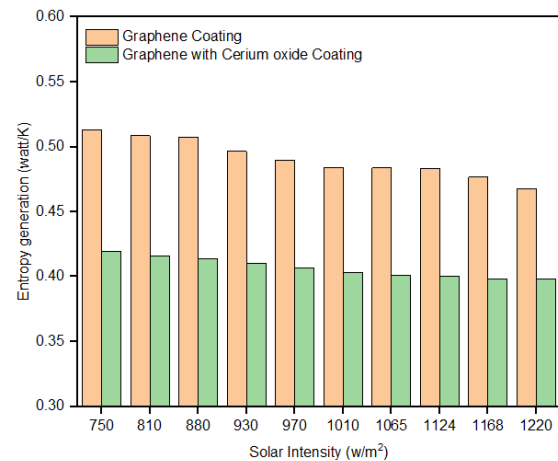

Fig. 9: Variation of solar intensity vs entropy generation

Fig. 10 depicts the variation of exergy analysis with solar intensity; exergy analysis is required to understand the basic design and performance of any thermal system. Within all conditions of the experimental investigation, the exergy efficiency followed the change in instantaneous production or absorbed energy. When the sun intensity was 750 w/m², the minimal exergy efficiency values were reached, and as the solar intensity increased,

the exergy efficiency improved. The exergy efficiency of graphene and hybrid nanomaterial coatings on absorber plates is 1.88 percent and 2.32 percent, respectively. Furthermore, the exergy efficiency of the hybrid coating absorber surface is higher than that of the graphene coating on the absorber plate, since the hybrid coating absorber plate has the largest heat transfer rate.
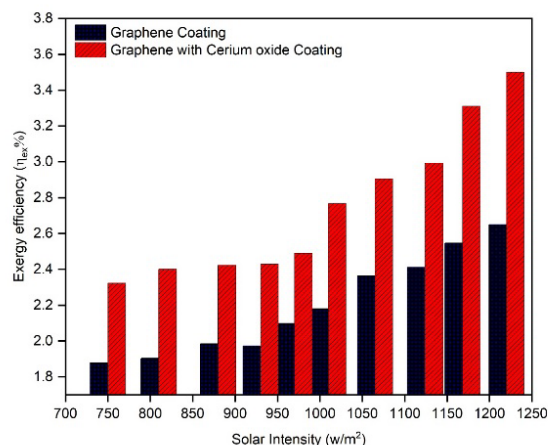

Fig. 10: Variation of exergy efficiency vs solar intensity

Fig. 11 shows the temperature variation in TSAH with hybrid coating on absorber plate. The profile of air temperature variation via this triangle duct is depicted in the picture for a better understanding of the roughened absorber plate TSAH's airflow thermal performance. As the sun's intensity rises, the temperature within the duct rises, with the highest temperature at the TSAH's entrance point of length L=0.2 m. At L=0.8 m, the temperature inside the duct is at its lowest. The temperature of the air stream is related to the intensity of solar radiation, indicating that the air stream can reach a higher temperature with more direct solar radiation.
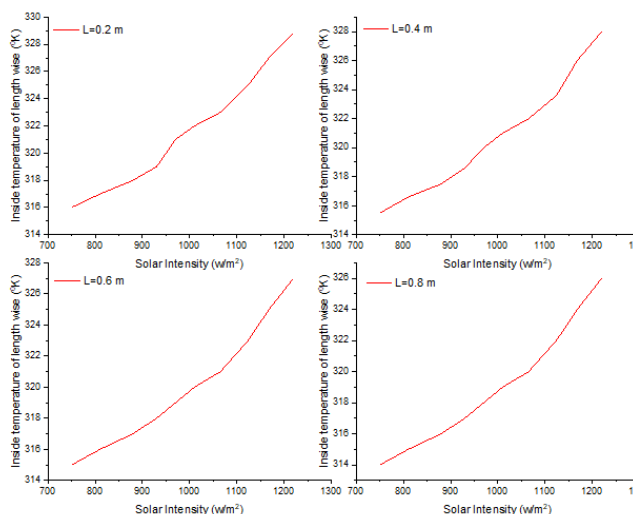

Fig. 11: Temperature variation in TSAH with hybrid coating on absorber plate

Fig. 12 depicts the change of intake and exit temperature in both situations as a function of solar intensity for the roughened absorber plate TSAH. The triangle duct solar air heater has the greatest temperature difference when compared to other SAH systems. Heat transfer between the airflow and the absorber surface-enhanced as a consequence. As the sun intensity rises, the hybrid coated absorber plate's output temperature goes up.
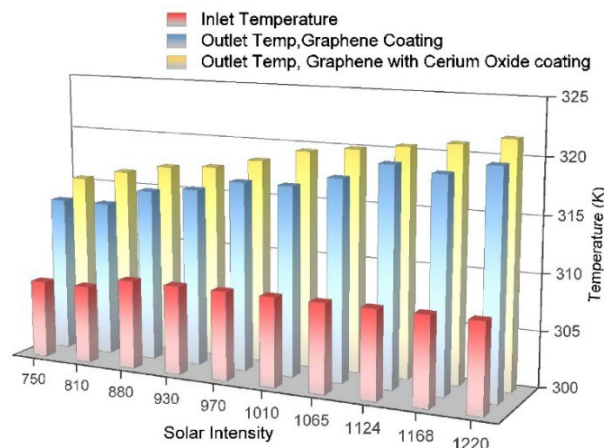

Fig. 12: Variation of inlet and outlet Temperature

5. Conclusions

The TSAH performance is compared to graphene and a hybrid coating embedded in black paint. The TSAH produces hot air for space heating and drying purpose. Based on the input parameters analysed and the experimental results obtained in comparison to both types of coating on the absorber plate. The following is a brief description of the findings:

- The graphene/CeO$_2$-black paint coating on the TSAH absorber plate has a thermal efficiency of 3.56% greater than a graphene-black paint coating sun intensity ranges from 750 to 1220 W/m^2.
- The average exergy efficiency has increased by 0.55% as compared to the graphene-black paint coating on the absorber plate. Furthermore, as the sun's intensity rises. It is observed in the current research, the hybrid nanomaterial coating plays a significant role in improving the system's thermal and exergetic efficiency.
- Entropy generation is more for 2% graphene-black paint and minimum for 2% graphene/CeO$_2$-black paint on the absorber plate.
- The graphene/CeO$_2$-black paint on the absorber plate gives a higher outlet temperature compared to the graphene-black paint coating.

Nomenclature

A_e	Edge area
A_c	Glass plate area
A_p	Absorber plate area
D_h	Hydraulic Diameter of triangular section
h_w	Heat transfer coefficient of air
I	Solar Intensity
E_s	Net exergy energy rate
E_n	Surface gains exergy
E_{opt}	Optical exergy destructions
E_{abs}	Absorber plate exergy destructions
E_{env}	Envoimental exergy destructions
E_{ht}	Heat transfer exergy destructions
E_f	Friction exergy destructions
F'	Plate efficiency factor
F_R	Prandtl Number
P_r	Reynolds number
R_e	Nusselt number
N_u	Pumping power
P_m	Total loss component
U_L	Edge loss coefficient
U_e	Bottom loss coefficient
U_b	
U_t	
FESEM	Field Emission Scanning Electron Microscope
SAH	Solar air heater
TSAH	Triangular Solar air heater

Greek symbols

μ	The viscosity of the fluid
σ	Stefan Boltzmann constant
$\tau\alpha$	Product absorptivity and transmitivity
η_{th}	Thermal efficiency
η_{ex}	Exergy efficiency
ρ	Density of Air
ϵ_p	An emissivity of absorbing plate
ϵ_g	An emissivity of the glass cover

References

1) A. Berisha and L. Osmanaj, "Kosovo Scenario for Mitigation of Greenhouse Gas Emissions from Municipal Waste Management," EVERGREEN Joint Journal of Novel Carbon Resource Sciences & Green Asia Strategy, vol. 8, no. 3, pp. 509–516.

2) V. Gupta and A. Jayant, "A novel hybrid MCDM approach followed by fuzzy DEMATEL-ANP-TOPSIS to evaluate Low Carbon Suppliers," EVERGREEN Joint Journal of Novel Carbon Resource Sciences & Green Asia Strategy, vol. 8, no. 3, pp. 544–555.

3) I. Roihan, T. A. Kynan, E. A. Setiawan, and R. A. Koestoer, "Installing and Testing the Grashof Portable Incubator Powered Using the Solar Box 'Be-Care' for Remote Areas without Electricity," EVERGREEN Joint Journal of Novel Carbon Resource Sciences & Green Asia Strategy, vol. 7, no. 4, pp. 621–628.

4) S. K. Verma, N. K. Gupta, and D. Rakshit, "A comprehensive analysis on advances in application of solar collectors considering design, process and working fluid parameters for solar to thermal conversion," Solar Energy, vol. 208, pp. 1114–1150, Sep. 2020, doi: 10.1016/j.solener.2020.08.042.

5) R. Kumar and S. K. Verma, "Numerical investigation of performance analysis of Triangular Solar air heater using Computational Fluid Dynamics (CFD)," IOP Conf. Ser.: Mater. Sci. Eng., vol. 1116, no. 1, p. 012047, Apr. 2021, doi: 10.1088/1757-899X/1116/1/012047.

6) R. Kumar and S. K. Verma, "Review based on the absorber plate coating for solar air heater applications," IOP Conf. Ser.: Mater. Sci. Eng., vol. 1116, no. 1, p. 012053, Apr. 2021, doi: 10.1088/1757-899X/1116/1/012053.

7) A. K. Pandey et al., "Energy, exergy, exergoeconomic and enviroeconomic (4-E) assessment of solar water heater with/without phase change material for building and other applications: A comprehensive review," Sustainable Energy Technologies and Assessments, vol. 45, p. 101139, Jun. 2021, doi: 10.1016/j.seta.2021.101139.

8) R. Pandey and M. Kumar, "Efficiencies assessment of an indoor designed solar air heater characterized by V baffle blocks having staggered racetrack-shaped perforation geometry," Sustainable Energy Technologies and Assessments, vol. 47, p. 101362, Oct. 2021, doi: 10.1016/j.seta.2021.101362.

9) H. S. Arunkumar, K. Vasudeva Karanth, and S. Kumar, "Review on the design modifications of a solar air heater for improvement in the thermal performance," Sustainable Energy Technologies and Assessments, vol. 39, p. 100685, Jun. 2020, doi: 10.1016/j.seta.2020.100685.

10) D. Jeong et al., "Absorption mechanism and performance characterization of CuO nanostructured

absorbers," Solar Energy Materials and Solar Cells, vol. 169, pp. 270–279, 2017, doi: https://doi.org/10.1016/j.solmat.2017.05.029.

11) Z. Chen and T. Boström, "Electrophoretically deposited carbon nanotube spectrally selective solar absorbers," Solar Energy Materials and Solar Cells, vol. 144, pp. 678–683, 2016, doi: https://doi.org/10.1016/j.solmat.2015.10.016.

12) E. Wäckelgård et al., "Development of W–SiO2 and Nb–TiO2 solar absorber coatings for combined heat and power systems at intermediate operation temperatures," Solar Energy Materials and Solar Cells, vol. 133, pp. 180–193, 2015, doi: https://doi.org/10.1016/j.solmat.2014.10.022.

13) E. Šest, G. Dražič, B. Genorio, and I. Jerman, "Graphene nanoplatelets as an anticorrosion additive for solar absorber coatings," Solar Energy Materials and Solar Cells, vol. 176, pp. 19–29, 2018, doi: https://doi.org/10.1016/j.solmat.2017.11.016.

14) R. Kumar, S. K. Verma, and M. Singh, "Experimental investigation of nanomaterial doped in black paint coating on absorber for energy conversion applications," Materials Today: Proceedings, Dec. 2020, doi: 10.1016/j.matpr.2020.11.006.

15) J. E. Nady, A. B. Kashyout, S. Ebrahim, and M. B. Soliman, "Nanoparticles Ni electroplating and black paint for solar collector applications," Alexandria Engineering Journal, vol. 55, no. 2, pp. 723–729, 2016, doi: https://doi.org/10.1016/j.aej.2015.12.029.

16) R. Kumar, S. K. Verma, and V. Sharma, "Performance enhancement analysis of triangular solar air heater coated with nanomaterial embedded in black paint," 2020, doi: 10.1016/j.matpr.2020.02.538.

17) R. Kumar and S. K. Verma, "EXERGETIC AND ENERGETIC EVALUATION OF AN INNOVATIVE SOLAR AIR HEATING SYSTEM COATED WITH GRAPHENE AND COPPER OXIDE NANO-PARTICLES," Journal of Thermal Engineering, vol. 7, no. 3, Art. no. 3, Feb. 2021, doi: 10.18186/thermal.887023.

18) T. K. Abdelkader, Y. Zhang, E. S. Gaballah, S. Wang, Q. Wan, and Q. Fan, "Energy and exergy analysis of a flat-plate solar air heater coated with carbon nanotubes and cupric oxide nanoparticles embedded in black paint," Journal of Cleaner Production, vol. 250, p. 119501, 2020, doi: https://doi.org/10.1016/j.jclepro.2019.119501.

19) J. A. Duffie and William A. Beckman, Solar Engineering of Thermal Processes, Fourth Edition. 2013.

20) S. K. Verma, A. K. Tiwari, and D. S. Chauhan, "Experimental evaluation of flat plate solar collector using nanofluids," Energy Conversion and Management, vol. 134, pp. 103–115, 2017, doi: https://doi.org/10.1016/j.enconman.2016.12.037.

21) N. Akhtar and S. C. Mullick, "Approximate method for computation of glass cover temperature and top heat-loss coefficient of solar collectors with single glazing," Solar Energy, vol. 66, no. 5, pp. 349–354, Aug. 1999, doi: 10.1016/S0038-092X(99)00032-8.

22) T. K. Abdelkader, Y. Zhang, E. S. Gaballah, S. Wang, Q. Wan, and Q. Fan, "Energy and exergy analysis of a flat-plate solar air heater coated with carbon nanotubes and cupric oxide nanoparticles embedded in black paint," Journal of Cleaner Production, p. 119501, Nov. 2019, doi: 10.1016/j.jclepro.2019.119501.

23) S. A. Klein, "Calculation of the monthly-average transmittance-absorptance product," Solar Energy, vol. 23, no. 6, pp. 547–551, Jan. 1979, doi: 10.1016/0038-092X(79)90083-5.

24) S. A. Klein, "Calculation of flat-plate collector loss coefficients," Solar Energy, vol. 17, p. 79, Apr. 1975, doi: 10.1016/0038-092X(75)90020-1.

25) K. Nidhul, S. Kumar, A. K. Yadav, and S. Anish, "Enhanced thermo-hydraulic performance in a V-ribbed triangular duct solar air heater: CFD and exergy analysis," Energy, vol. 200, p. 117448, 2020, doi: https://doi.org/10.1016/j.energy.2020.117448.

26) E. B. Wylie, V. L. Streeter Fluid transients. New York.: McGraw-Hill., 1978.

27) R. W. Bliss, "The derivations of several 'Plate-efficiency factors' useful in the design of flat-plate solar heat collectors," Solar Energy, vol. 3, no. 4, pp. 55–64, Dec. 1959, doi: 10.1016/0038-092X(59)90006-4.

28) S. A. Kalogirou, Solar Energy Engineering: Processes and Systems. Academic Press, 2013.